DNA molecules deviate from shortest trajectory when driven through hydrogel

Juan Guan, Kejia Chen, Ah-Young Jee, and Steve Granick

Citation: The Journal of Chemical Physics **149**, 163331 (2018); doi: 10.1063/1.5033990
View online: https://doi.org/10.1063/1.5033990
View Table of Contents: http://aip.scitation.org/toc/jcp/149/16
Published by the American Institute of Physics

DNA molecules deviate from shortest trajectory when driven through hydrogel

Juan Guan,[1,2] Kejia Chen,[3] Ah-Young Jee,[1] and Steve Granick[1,4]
[1]*Center for Soft and Living Matter, Institute for Basic Science (IBS), Ulsan 44919, South Korea*
[2]*Department of Pharmaceutical Chemistry, University of California, San Francisco, San Francisco, California 94143, USA*
[3]*Google, Inc., Mountain View, California 94043, USA*
[4]*Department of Chemistry, Ulsan National Institute of Science and Technology (UNIST), Ulsan 44919, South Korea*

(Received 8 April 2018; accepted 17 July 2018; published online 6 August 2018)

Dynamic fluorescence-based single-molecule imaging of λ-DNA molecules driven through agarose hydrogels by DC electric fields reveals that passage through the hydrogel (98.5% water content) induces mobility orthogonal to the external field. Tortuous paths followed by the DNA molecules, which are heavily entangled in the hydrogel mesh as their contour length is nearly 100 times the hydrogel mesh size of 200 nm, cause them to appear to diffuse orthogonal to the driving force. The higher the driving field, from 2 to 16 V/cm, the higher the off-axis dispersion is, over the same time interval. We measure the off-axis displacement distribution over 3 orders of magnitude of probability density and find a master curve after normalizing for time (t) elapsed, but the power of time for normalizing increases with the external field, from $t^{0.25}$ to $t^{0.6}$ with increasing field. Comparing trajectories over the same distance traveled in the electric field direction, we observe whereas for the highest field strengths DNA molecules come closest to taking the shortest trajectory between two points in space, deviations from the shortest trajectory grow larger and larger (up to 40% larger) as one approaches the case of small yet finite external field strength. *Published by AIP Publishing.*
https://doi.org/10.1063/1.5033990

INTRODUCTION

Dispersion (beyond what can be attributed to Brownian motion) of the paths of moving objects owing to an inhomogeneous medium is common in nature. Beyond its numerous examples and applications in the context of wave scattering, for example, in wave optics and ultrasound, here we are concerned with the more general problem of understanding the path of moving particles that must turn around objects because resistance to their motion is inhomogeneous in space. Such dispersion of moving objects involves flow through porous media,[1–3] bacteria chemotaxis,[4,5] intruder objects driven through granular materials,[6,7] and cellular transport of vesicles.[8] Also, dispersion transverse to the direction of net motion (beyond what can be attributed to Brownian motion) presents a design constraint in mixing and de-mixing streams of fluids in reactors,[9] efficient separation in chromatography,[10,11] and transport through cellular cytoskeleton meshes or other crowded environments.[12,13] A vast literature largely considers the ensemble-averaged behavior resulting from multiple scattering events. Here we are concerned instead with single molecules and with the situation when a given trajectory has only a limited amount of scattering. Between the limits of no scattering on the one hand, and fully developed randomized motion that produces isotropic[14] or localized[15] scattering, the situation considered here is the middle ground.

We report, based on single-molecule fluorescence imaging of individual molecules, that when DNA undergoes directed transport through a hydrogel, a considerable number of the moving molecules take paths longer than the shortest geometrical path. Dispersion of DNA under electrophoresis has been known previously in the context of technology to improve electrophoretic separation efficiency by the pulsed electric field[16–19] but, to our knowledge, not previously when the driving electric field is DC in a single direction. Reasons are given to expect such behavior to be common for linear macromolecules in porous media that contain a multiplicity of alternative transport paths, the traversal of which involves dissipation of nearly degenerate energy.

From imaging hundreds of individual λ-DNA molecules driven through agarose hydrogel network, we conclude that the footprint of a chain follows a tortuous path, effectively described as successive discrete dispersion events at defined turning points. The hydrogel network presents fixed obstacles that force the moving molecules to go around and between the hydrogel strands. As compared to other transport systems that exhibit transverse motion, interpretation in the present system is relatively simple because these networks cannot rearrange, being crosslinked. In contrast to the voluminous literature that previously studied ensemble-averaged DNA transport along the external force direction,[20,21] this study focuses upon off-axis mobility. Counter-intuitively, there is mobility in directions along which there was no driving force from the external field.

MATERIALS AND METHODS

The methods of sample preparation and agarose gel preparation are described in detail in an earlier publication from this laboratory.[22] Briefly, the λ-DNA chains, covalently labeled uniformly along the chain with fluorescence dyes, were tracked while they were driven through the optically transparent agarose network by an externally applied DC electric field. Trace amounts of the DNA chains were embedded in the agarose gel network to ensure single-molecule tracking and negligible inter-chain contacts between DNA chains. It is known that gravity has negligible effect on the DNA chains[23] and the current work focuses on their motion in the x-y plane.

Fluorescence microscopy

Data were acquired using an optical microscope in epifluorescence mode, typically at the frame rate 33 fps. A 532 nm excitation laser was focused at the rear focal point of an oil immersion objective (Zeiss, α-Plan Fluor 100×, numerical aperture NA = 1.45) with 2.5× post-magnification to image with a resolution of 64 nm × 64 nm/pixel.

Fluorescence images were collected through the same objective and detected by a back-illuminated electron multiplying charge-coupled device (EMCCD) camera (Andor iXon DV-897 BV) after filtering out light from the excitation laser. The movies were converted into digital format and analyzed. A typical dataset consists of 30 movies at one field condition, each of them consisting of 4000 frames per movie acquired at 33 fps. The resulting dataset of $>10^4$ conformations was collected from images of thousands of molecules.

Gel preparation

Single-molecule measurements of DNA chain conformations were made in a miniature gel electrophoresis setup using agarose gel [final concentration 1.5% (w/v)] in 0.5× TBE buffer, i.e. a mixture of 45 mM Tris, 45 mM borate, 1 mM EDTA, ethylenediaminetetraacetic acid, the DNA being at picomolar concentration. The anti-photobleaching agent, ascorbic acid (Sigma-Aldrich), was present at a final concentration of 10 mM. The grade of agarose (Fisher, molecular biology grade, low EEO, endosmosis) was selected where cationic moieties were added to balance the native anionic moieties in the agarose gel. A DC voltage was applied across two Pt electrodes to generate an electric field ranging from 2 to 16 V/cm.

DNA labeling

λ-DNA (monodisperse with precisely 48 502 bp in its length, Promega) was labeled by covalently attaching a dye, a rhodamine B derivative (Mirus Bio) to heteroatoms on DNA, at a labeling density of roughly one dye per 5 base pairs. Covalent attachment eliminates the extension of the contour length that results from using conventional intercalated dyes.

Identification of turning points in single-molecule trajectories

As the path a migrating chain follows inside a gel is tortuous, although a constant force is applied to the chain, we identified turning points, thus removing noise from the raw data while keeping the orientation information, as illustrated in Fig. 1(a). The analysis of individual scattering events is based on identification of turning points. To define turn-to-turn steps, we used the error radius method documented in the literature.[8,24,25] In this method, a straight line connects two points along the trajectory; then one end of it extends to subsequent data points considered sequentially, until the data points in between start to deviate from the line above a threshold. The final end point is identified as a turning point and is used to initiate a new line. The threshold for

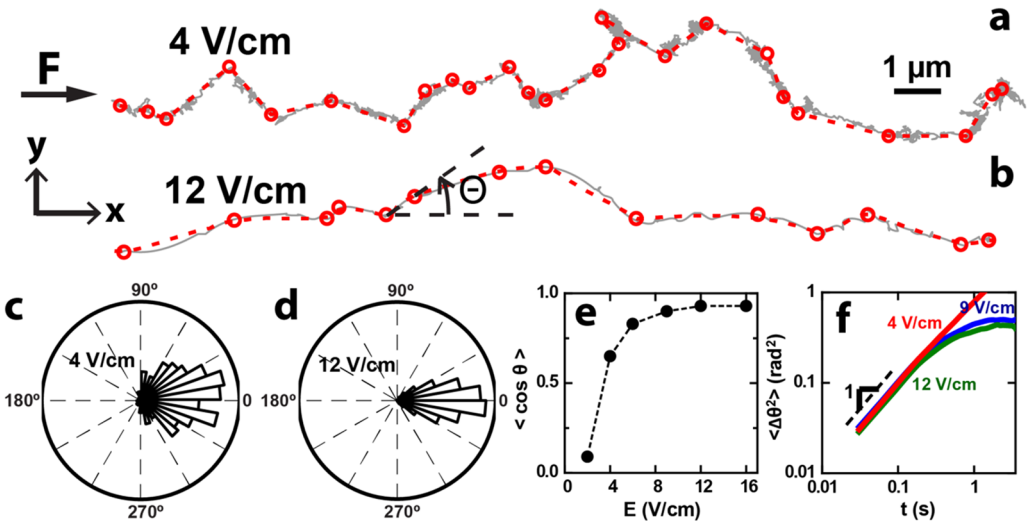

FIG. 1. Tortuous paths of DNA chains driven through hydrogel. Representative trajectories compared at field strengths 4 V/cm (a) and 12 V/cm (b) show actual measurements (gray) and the turning points identified by analysis (red). Dotted red line shows interpolated lines between turning points. Higher field leads to a straighter and less tortuous path. There is extensive off-axis (y) displacement though the driving field which is in the x direction. Angle between motion and field direction is denoted as θ. Histogram of θ distribution on a circular plot, plotted for 4 V/cm (c) and 12 V/cm (d). (e) Mean value of cos θ is plotted against increasing field strength, E. (f) Mean squared angle displacement is plotted against time for field strengths 4, 9, and 12 V/cm. The dotted line with 1 compares to the expectation for Fickian diffusion.

each trajectory is adapted to the end-to-end distance of that particular trajectory to account for the heterogeneity between trajectories. The threshold converges when the turning angles become uncorrelated and distributed isotropically. About 1×10^6 images are acquired in each network for statistical analysis.

RESULTS

The average network mesh size was estimated for agarose at this 1.5 wt. % concentration (~200 nm).[21,26–29] Comparison to λ-DNA (~16 μm contour length, ~50 nm persistence length[30]) implies that the average chain threads at rest through dozens of meshes (~20-40 meshes) of the network. Additionally, at large voltages, the stretched chains would be even more threaded than at equilibrium. Its large size, much exceeding the diffraction limit ~0.3 μm, allows facile fluorescence imaging. As a previous study in this laboratory showed that under these experimental conditions a driven DNA chain follows the path of its leading end,[22] we tracked the center-of-mass of each of these driven molecules. As the Brownian motion of these molecules over the time scale of these experiments was essentially trapped in the agarose gel, all motions analyzed here originated in driven motion.

The footprint of a migrating chain traces a tortuous path though the applied electric force which is constant, as illustrated by the gray tracks in a representative image, Figs. 1(a) and 1(b). The overall chain motion is in the force direction, but over the course of doing so, the center of mass can zig and zag orthogonal to the force direction, with a zig-zag length scale a few times the average network mesh size. To quantify the orientation bias and its dynamics, first we identify turning points along the track at which large direction changes occur, denoted by red dots in Figs. 1(a) and 1(b). Overlay with the original track confirms that these turning points follow the evolution of chain orientation. In other words, the motion can be described effectively as successive individual dispersion events at defined turning points that deflect the otherwise straight and directed driven motion.

Interestingly, transverse motion differs distinctively between the cases of high and low applied voltage. At low field (6 V or less), the chain motion is often at a notable angle to the force and shows frequent local motion along the track and occasional backward motion against the force direction. By contrast, at the highest field, the motion is more directed with a straighter and smoother track showing less local or backward motion. These differences suggest that some paths in the network inaccessible to a chain at low field become available at high field as higher field might allow a chain to channel through narrow constrictions in the network more easily, though the agarose network itself could reconfigure in response to high electric fields.[31–33]

The angle between motion and field direction, calculated from the turning points and their distribution, is plotted as a histogram on a circular plot in Figs. 1(c) and 1(d). Consistent with the transverse dispersion just noted, the angle at low field is more spread out with respect to the field direction and displays a wider distribution across the first and fourth quadrants, as well as occasional backward motion as represented in the second and third quadrants. By contrast, the angle at high field is narrowly distributed in the small-angle region in the first and fourth quadrants and displays almost no backward angles. By adjusting the field strength, the average orientation was tuned over a wide range as $\cos\theta$ increased monotonically with field strength between 0 (isotropic) and 1 (perfect alignment), as plotted in Fig. 1(e). The mean squared angular displacement [Fig. 1(f)] was initially diffusive, consistent with dynamics of a generic rotator undergoing a rotational random walk, and gradually reached a plateau at long time, consistent with the orientation bias exerted by the field. The difference between high and low field lies in the bias level, the higher field leading to a stronger orientation bias and lower plateau level. A curious feature is that no discernible difference was observed in the initial diffusive regime according to the field magnitude. This suggests a base level of angle fluctuation due to thermal Brownian motion.

Since the turning points identify individual dispersion events, we measured the transverse displacement perpendicular to the field between these individual dispersion events. These were distributed exponentially with a characteristic length [Fig. 2(a)]. Interestingly, the distribution was the same, with the same decay length, regardless of whether the field

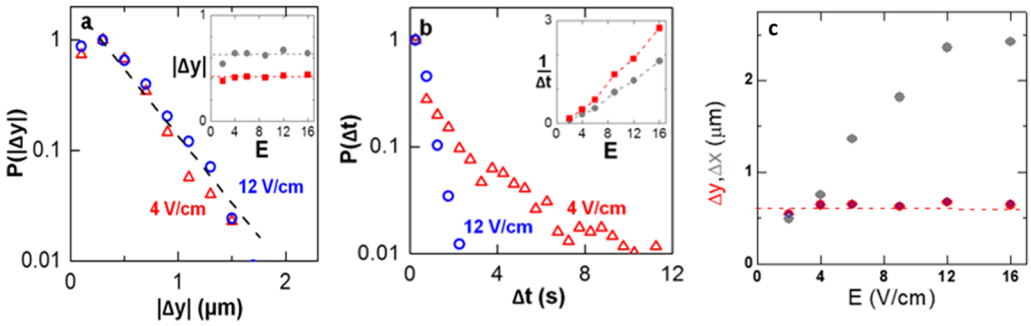

FIG. 2. Transverse displacement distributions between successive turning points (in transverse direction) of trajectories illustrated in Fig. 1. (a) Probability distribution of transverse displacement |Δy| between discrete dispersion events identified, as illustrated in Figs. 1(a) and 1(b). The linear dashed line is a guide to the eye. (*Inset*) Mean transverse displacement |Δy| in units of μm is plotted as a function of electric field E in V/cm evaluated relative to turning points (squares) and to switches of direction (circles). (b) Waiting time distribution between discrete dispersion events identified as illustrated in Figs. 1(a) and 1(b). (*Inset*) Mean scattering frequency in units of s^{-1} plotted as a function of electric field E in units of V/cm. Symbols are the same as in (a). (c) Comparison of the mean transverse (|y|) and longitudinal (|x|) displacements between successive turning points of trajectories, plotted against the magnitude of the external field.

strength was high or low [Fig. 2(a), inset]. This length scale is comparable to the network mesh size, suggesting that the network structure might determine the location of chain dispersion and the magnitudes of transverse fluctuations. We note that although the agarose gel is known to have large spatial heterogeneity, at the ensemble level averaged over sufficient length scale and time scale, the chains are scattered with an effective characteristic rate constant, similar to many other random walk processes such as run-and-tumble of bacteria with a turning rate or even a generic 1D random walker that switches direction at a certain rate.[34] Indeed we find the waiting time between individual dispersion events to be exponential, which is consist with a stochastic interpretation of chain dispersion [Fig. 2(b)]. Interestingly, the scattering frequency increased with increasing field. Since the transport mobility of a driven chain is known to accelerate with increasing field,[20,21] the increased scattering frequency likely reflects faster encounters with obstructing network strands. This in turn suggests that the electric field acts like an effective elevated temperature to promote dispersion by increasing the scattering frequency, though we are careful not to imply that there is an elevated "temperature" in the thermodynamic sense of the word.[35]

As a consistency check, we also analyzed the switching rate, defined as the subset of turning points that switch between +y and −y direction relative to driven motion in the +x direction. The exponential distribution of distance and waiting time between individual events and general trend with field were confirmed [Figs. 2(a) and 2(b)]. Comparing the mean transverse displacement between successive turning points to the direction traversed in the field direction [Fig. 2(c)], one sees that while their magnitude is similar when the field is low, with increasing field the transverse component remains constant while the other component rises. This implies that whereas the DNA molecules came closest to taking the shortest trajectory between two points in the case of highest electric fields, deviations from the shortest trajectory were larger and larger as one approached the case of a small but finite field. Simple Pythagorean-type considerations imply that the length of actual trajectory of individual molecules exceeded the shortest distance by the average factor of between 1.1 (highest field) and 1.4 (low field). To understand the orientation bias in the context of the entropic barrier, whereas the entropic barrier in the transverse direction is comparable to thermal energy kT regardless of external electric field, the entropic barrier along the field direction decreases drastically with field as approximately inverse of the electric field,[36] leading to a large difference in motion in the two directions at high fields. For instance, we show that only at the lowest field explored (2 V/cm), the transverse motion is comparable to the longitudinal motion [Fig. 2(c)] and we already start to see orientation bias at 4 V/cm. Therefore the effective entropic barrier is close to thermal energy kT at 2 V/cm and less than kT (~1/8 to 1/4 kT) at 16 V/cm. Note that the current analysis of turning points parallels the usual highly averaged analysis such as persistence length and angular mean square displacement. However, although those averaged quantities manifest smoothly varying changes [such as the smooth angular mean-square displacement curves shown in Fig. 1(f)], the current analysis using single-molecule tracking shows that turning points, points of high curvature in the trajectory, truly do exist at the microscopic level. In addition, the difference between transverse and longitudinal directions would be lost in the persistence length or angular mean square displacement analysis, in contrast to highlighting the difference in mean transverse and longitudinal displacements between successive turning points of trajectories [Fig. 2(c)].

The force-enhanced dispersion normal to the driving force is evident when one plots the variance of transverse displacement against time for different field conditions [Fig. 3(a)]. For a given time interval, the variance at low field is similar to that without field, but dispersion is considerably enhanced as the field increases to high. The acceleration of transverse dispersion by the field is further confirmed by observing a wider distribution of transverse displacement at higher field for a given time interval [Fig. 3(a), inset]. This transverse dispersion increases by orders of magnitude with increasing field strength and does not saturate. Curiously, the limited theoretical predictions for this problem predict a lesser effect.[19]

With the elapsed time, spread in the off-axis direction increases such that the increase of variance with time is approximately linear [Fig. 3(a)]. However, closer inspection of this data on log-log scales [Fig. 3(b)] reveals that rather than

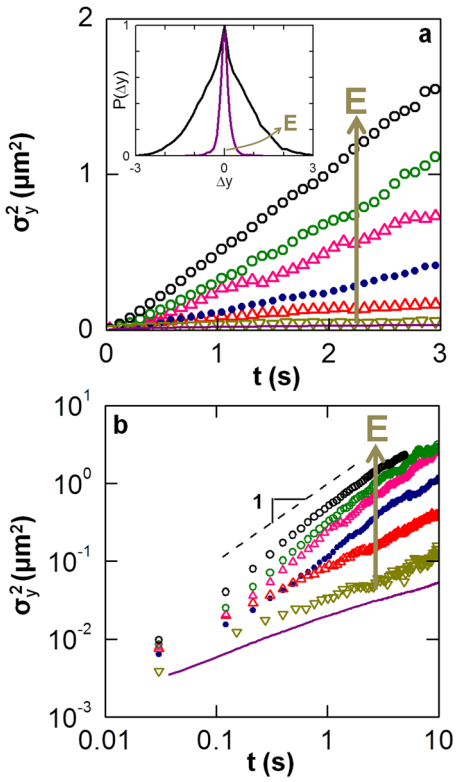

FIG. 3. Variance of transverse displacement σ_y^2 as a function of time elapsed. (a) Plot of these quantities on linear scales. Without the electric field, $\sigma_y^2 \approx 0$ (purple line). Symbols from bottom to top are 2, 4, 6, 9, 12, and 16 V/cm. (*Inset*) Probability distribution of Δy, in units of μm, after 1.5 s elapsed time for drive fields 2 and 16 V/cm (inner and outer curves, respectively), after normalizing these distributions to their maxima. (b) Log-log plots of the data in panel (a) showing a slope of 1 as a guide to the eye.

following strict Fickian diffusion, the variance is slightly sub-diffusive (scaling exponent < 1) at low field and super-diffusive (scaling exponent > 1) at higher field. It is known that diffusive dynamics of transverse motion might be expected from stochastic multiple dispersion events[37] as diffusion can arise from directed motion that changes direction by stochastic rotation and this is observed in simulations of transverse motion of driven particles in granular materials.[38,39] In fact, we find that simulated 1D random walk trajectories with constant speed and exponentially distributed time between direction switching events matching experimental values would predict Fickian spreading in the off-axis direction. That we saw this tendency but did not observe it to hold quantitatively suggests that transverse motion may couple to the direction of driven motion.

These large datasets also allow us to scrutinize the probability distribution of transverse displacement and how they scale with elapsed time. Plotted over 3 decades of probability density, this is shown in Fig. 4(a). Consistent with the time-dependence of the variance (Fig. 3), the distribution spreads with increasing time at a given field strength and the distributions at different field strengths approximately collapse with the scaled time. For example, the displacement distributions at 6 V/cm overlap when scaled by $t^{0.5}$ [Fig. 4(b)], suggesting diffusive transverse motion with the same form of displacement distribution.[40–42] But as over a broader range of field strength, the transverse motion fails to follow a simple diffusion (Fig. 3); in order to achieve collapse across a wider range of field strength, the time scaling must be varied, $t^{0.25}$ to $t^{0.6}$ [Figs. 4(c) and 4(d)], consistent with sub-diffusive motion at low field and super-diffusive motion at high field.

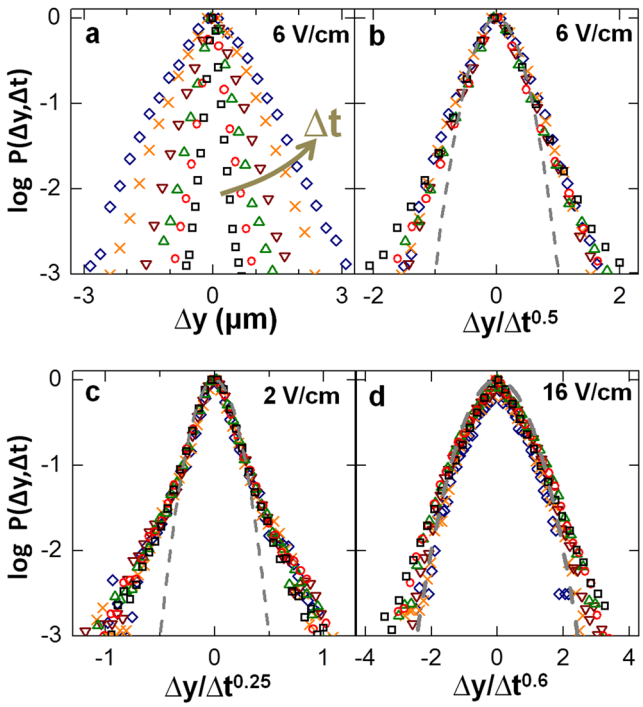

FIG. 4. Transverse displacement distributions evolving with elapsed time. (a) These distributions, normalized to their respective maxima and plotted on semi-log scales, are shown at time intervals 0.1, 0.3, 0.6, 1.2, 2.4, and 3.6 s (squares, circles, up-triangles, down-triangles, crosses, and diamonds, respectively). (b) The goodness of the fit onto an apparent master curve, for field strength 6 V/cm, upon normalizing the abscissa as $\Delta y/\Delta t^{0.5}$. (c) The goodness of the fit onto an apparent master curve, for field strength 2 V/cm, upon normalizing the abscissa as $\Delta y/\Delta t^{0.25}$ [symbols same as in panel (a)]. (d) The goodness of the fit onto an apparent master curve, for field strength 16 V/cm, upon normalizing the abscissa as $\Delta y/\Delta t^{0.6}$. Symbols in all panels are the same as in panel (a). All the master curves have central portions consistent with Gaussian behavior (dashed line) but heavy tails at larger displacements showing strong deviation from Gaussian behavior in this regime, except for the case of the highest drive field, where deviations from Gaussian behavior are the smallest.

The shapes of these distributions significantly deviate from classical Gaussian expectation and show a heavy tail implying the existence of a large subpopulation with large transverse displacements [Figs. 4(b)–4(d)]. This heavy tail is qualitatively reminiscent of dynamic heterogeneity in supercooled and glassy systems, but as the underlying physical origin must differ, this similarity is considered to be only phenomenological. Here, instead of reflecting collective motion of a cluster of relatively mobile particles,[43–45] the faster subpopulation probably reflects the fact that the network environment is heterogeneous, even on length scales an order of magnitude larger than the mesh size, and that it contains some regions which comprise effective channels favoring transverse chain motion with respect to the force direction.[46] Non-Gaussian distributions, recently observed in many diverse soft matter systems, are conjectured to originate from insufficient averaging of spatial and temporal heterogeneity.[41] In this experimental system, to find the distribution closest to Gaussian at highest field strength may suggest that the channeling effect of a subpopulation of chains is least important when the field is the highest. More simply, it is also consistent with the scenario that in this situation the driven chains experience the most collisions, thus most fully randomizing their transverse motion.

It is reasonable physically to anticipate that dispersion resulting from collisions and steric impediments encountered by these chains driven through gels may extrapolate to other driven systems. Among these are not only complex fluids and colloids[41–43] but also when a microenvironment is ordered such as by fabricated nanopost arrays.[47] This study considered the situation that strict rectilinear motion is prohibited, yet the number of collisions is insufficient to create well-developed off-axis diffusion. The likely underlying reason is probably roughly analogous to the light passage through smoke and other instances of multiple scattering. The field-enhancing effect reported here suggests a possible route to actively control dispersion dynamics normal to the transport direction, relevant to processes such as mixing, separation, and other transport through crowded environments.

ACKNOWLEDGMENTS

This work was supported by the Institute for Basic Science, project code IBS-R020-D1. J.G. and K.C. acknowledge support from the Department of Energy, Division of Materials Science, under Award No. DEFG02-02ER46019.

[1] C. Scholz, F. Wirner, J. R. Gomez-Solano, and C. Bechinger, Europhys. Lett. **107**, 54003 (2014).
[2] J. D. C. Jacob, R. Krishnamoorti, and J. C. Conrad, Phys. Rev. E **96**, 022610 (2017).

[3]A. Fiege, M. Grob, and A. Zippelius, Granular Matter **14**, 247–252 (2012).
[4]G. H. Wadhams and J. P. Armitage, Nat. Rev. Mol. Cell Biol. **5**, 1024–1037 (2004).
[5]T. Ahmed, T. S. Shimizu, and R. Stocker, Nano Lett. **10**, 3379–3385 (2010).
[6]D. Wang, Y. Yang, and W. Du, Powder Technol. **286**, 385–391 (2015).
[7]B. D. Texier, A. Ibarra, and F. Melo, PLoS One **12**, e0175412 (2017).
[8]K. Chen, B. Wang, and S. Granick, Nat. Mater. **14**, 589 (2015).
[9]T. K. Perkins and O. C. Johnston, Soc. Pet. Eng. J. **3**, 70–84 (1963).
[10]A. Daneyko, D. Hlushkou, S. Khirevich, and U. Tallarek, J. Chromatogr. A **1257**, 98–115 (2012).
[11]U. Tallarek, K. Albert, E. Bayer, and G. Guiochon, AIChE J. **42**, 3041–3054 (1996).
[12]C. K. Choi, J. D. Fowlkes, S. T. Retterer, P. Siuti, S. Lyer, and M. J. Doktycz, ACS Nano **4**, 3345–3355 (2010).
[13]P. Habdas, D. Schaar, A. C. Levitt, and E. R. Weeks, Europhys. Lett. **67**, 477–483 (2004).
[14]A. L. Crosbie and J. W. Koewing, J. Math. Anal. Appl. **57**, 91–109 (1977).
[15]D. S. Wiersma, Nat. Phys. **4**, 359–367 (2008).
[16]B. Tinland, Electrophoresis **17**, 1519–1523 (1996).
[17]L. Meistermann and B. Tinland, Phys. Rev. E **58**, 4801–4806 (1998).
[18]J. Boileau and G. W. Slater, Electrophoresis **22**, 673–683 (2001).
[19]M. G. Gauthier, G. W. Slater, and K. D. Dorfman, Eur. Phys. J. E **15**, 71–82 (2004).
[20]K. Dorfman, Rev. Mod. Phys. **82**, 2903–2947 (2010).
[21]J.-L. Viovy, Rev. Mod. Phys. **72**, 813–872 (2000).
[22]J. Guan, B. Wang, S. C. Bae, and S. Granick, J. Am. Chem. Soc. **135**, 6006–6009 (2013).
[23]D. E. Smith, T. T. Perkins, and S. Chu, Macromolecules **29**, 1372–1373 (1996).
[24]P. Turchin, *Quantitative Analysis of Movement: Measuring and Modeling Population Redistribution in Animals and Plants* (Sinauer Associates, Inc., 1998).
[25]D. M. de Jager, F. J. Weissing, P. M. J. Herman, B. A. Nolet, and J. van de Koppel, Science **332**, 1551–1553 (2011).
[26]J. Narayanan, J.-Y. Xiong, and X.-Y. Liu, J. Phys.: Conf. Ser. **28**, 83–86 (2006).
[27]G. A. Griess, K. B. Guiseley, and P. Serwer, Biophys. J. **65**, 138–148 (1993).
[28]A. Pluen, P. A. Netti, R. K. Jain, and D. A. Berk, Biophys. J. **77**, 542–552 (1999).
[29]B. H. Zimm and S. D. Levene, Q. Rev. Biophys. **25**, 171–204 (1992).
[30]G. S. Manning, Biophys. J. **91**, 3607–3616 (2006).
[31]D. L. Holmes and N. C. Stellwagen, J. Biomol. Struct. Dyn. **7**, 311–327 (1998).
[32]J. Stellwagen and N. C. Stellwagen, Biopolymers **34**, 187–201 (1994).
[33]J. Stellwagen and N. C. Stellwagen, J. Phys. Chem. **99**, 4247–4251 (1995).
[34]A. P. Solon, M. E. Cates, and J. Tailleur, Eur. Phys. J.: Spec. Top. **224**, 1231–1262 (2015).
[35]M. Han, J. Yan, S. Granick, and E. Luijten, Proc. Natl. Acad. Sci. U. S. A. **114**, 7513–7518 (2017).
[36]J. Han, S. W. Turner, and H. G. Craighead, Phys. Rev. Lett. **83**, 1688 (1999).
[37]J. R. Howse, R. A. L. Jones, A. J. Ryan, T. Gough, R. Vafabakhsh, and R. Golestanian, Phys. Rev. Lett. **99**, 048102 (2007).
[38]D. Winter, J. Horbach, P. Virnau, and K. Binder, Phys. Rev. Lett. **108**, 028303 (2012).
[39]C. F. E. Schroer and A. Heuer, Phys. Rev. Lett. **110**, 067801 (2013).
[40]B. Wang, S. M. Anthony, S. C. Bae, and S. Granick, Proc. Natl. Acad. Sci. U. S. A. **106**, 15160–15164 (2009).
[41]B. Wang, J. Kuo, S. C. Bae, and S. Granick, Nat. Mater. **11**, 481–485 (2012).
[42]J. Guan, B. Wang, and S. Granick, ACS Nano **8**, 3331–3336 (2014).
[43]P. Chaudhuri, L. Berthier, and W. Kob, Phys. Rev. Lett. **99**, 060604 (2007).
[44]E. R. Weeks, J. C. Crocker, A. C. Levitt, A. Schofield, and D. A. Weitz, Science **287**, 627–631 (2000).
[45]W. K. Kegel and A. van Blaaderen, Science **287**, 290–293 (2000).
[46]N. C. Stellwaen and E. Stellwagen, J. Chromatogr. A **1216**, 1917–1929 (2009).
[47]Z. Chen and K. D. Dorfman, Electrophoresis **35**, 654–661 (2014).